


Metallic silicon subhydrides at high pressures studied by *ab initio* calculationsKazutaka Abe *Research Institute of Electrical Communication, Tohoku University, 2-1-1 Katahira, Aoba, Sendai, Miyagi 980-8577, Japan*

(Received 30 November 2020; revised 6 April 2021; accepted 9 April 2021; published 28 April 2021)

High pressure properties of silicon subhydrides SiH, SiH₂, and SiH₃ are investigated and compared with those of SiH₄ by using *ab initio* methods. Although the subhydrides are thermodynamically unstable at lower pressures, SiH, SiH₂, and SiH₃ are found to be stabilized above 486, 386, and 430 GPa, respectively. The predicted phases of SiH, SiH₂, and SiH₃ have $Fm\bar{3}m$, $I4/mmm$, and $I4/m$ symmetries, respectively, and are metallic. The density of states suggests that the electronic states at the Fermi energy are more delocalized in the subhydrides than in SiH₄. This fact is well reflected in the superconducting transition temperature (T_c) estimated for SiH₂ and SiH₃. Indeed, T_c reaches 83 K in SiH₂ at 400 GPa and 88 K in SiH₃ at 450 GPa while that is 28 K in SiH₄ at 400 GPa. Although T_c of SiH₄ is expected to exceed 100 K above 503 GPa, the current capability of diamond anvil cells suggests that high- T_c silicon hydride is more likely to be attained experimentally in subhydrides.

DOI: [10.1103/PhysRevB.103.134118](https://doi.org/10.1103/PhysRevB.103.134118)**I. INTRODUCTION**

Dense metallic hydrogen was predicted to become a superconductor in 1968 [1], and the superconducting transition temperature (T_c) is expected to be quite high. The superconductivity in dense hydrogen is supposed to be driven by phonon mediated mechanism, where the suggested high T_c is attributable to the high Debye temperature originating from the light hydrogen mass and the strong electron-ion interaction owing to the lack of core electrons. After this theoretical work, it was pointed out that the same mechanism of high- T_c superconductivity should also be applicable to dense hydrides [2]. The validity of the predictions has been confirmed recently. In 2015, superconductivity of sulfur hydride was observed experimentally, where T_c reaches 203 K at 155 GPa [3], and the composition of the superconducting phase was reported to be SH₃ [4,5]. Then, in 2019, it was found that lanthanum hydride shows superconductivity with T_c of 260 K at 180 GPa [6] and 250 K at 170 GPa [7]. The superconducting phase is very hydrogen rich and thought to have the composition of LaH₁₀ [8,9]. In both SH₃ and LaH₁₀, the T_c values estimated by theoretical calculations [4,8] are consistent with the experiments [3,5–7]. This agreement suggests that the superconductivity indeed originates from phonon mediated mechanism.

Recent extensive studies of dense metallic hydrides, which started around the middle of the 2000s, were initiated chiefly by the works of Ashcroft [10,11]. The works suggested that metallization pressures of some hydrides actually lie within the reach of diamond anvil cells, proposing group-IV hydrides as promising candidate compounds. In particular, silane (SiH₄) attracted great interest and was investigated in detail theoretically [12–17] and experimentally [18–21]. According to the experiment by Eremets *et al.* [20], SiH₄ is transformed into a metal at 50 GPa, and shows superconductivity with $T_c = 17$ K both at 96 GPa and at 120 GPa. Contrastingly, Sun *et al.* [18] and Strobel *et al.* [21] reported that SiH₄

remains nonmetallic even above ~ 150 GPa. Although there exists such a disagreement between the experiments, one thing which is clear about SiH₄ is that very high T_c is not observed yet. In fact, most theoretical works suggest that T_c does not reach 40 K in SiH₄ [13,15,17]. One exceptional phase is the $C2/m$ SiH₄ proposed by Zhang *et al.* [16], where T_c was estimated to be 106.31 K at 610 GPa.

For boron [22], carbon [23], aluminium [24], and germanium [25,26], which are adjacent to silicon on the Periodic Table, several subhydrides are predicted to be stabilized thermodynamically at high pressures; here, subhydrides are supposed to mean the compounds whose hydrogen concentrations are lower than the typical compositions, namely, BH₃, CH₄, AlH₃, and GeH₄. Among the predicted subhydrides, BH, AlH, Al₂H, GeH₃, Ge₂H, and Ge₃H are metallic. Moreover, AlH [24] and GeH₃ [25] are expected to show superconductivity with higher T_c than AlH₃ and GeH₄, respectively. These findings tempt one to examine whether silicon subhydrides likewise become stable and show superconductivity at megabar pressures.

Thus, in this paper, SiH, SiH₂, and SiH₃ are investigated by using *ab initio* methods. One of the well-known silicon subhydrides is disilane (Si₂H₆), and the high-pressure properties of disilane (or, strictly, SiH₃) were already investigated by using *ab initio* calculations [27,28]. The theoretical works on SiH₃ proposed $P\bar{1}$, $Pm\bar{3}m$, $C2/c$, and $Cmcm$ structures, and the $Pm\bar{3}m$ phase was shown to have the highest T_c (139 K at 275 GPa). As already suggested by Cui *et al.* [17], all these SiH₃ phases are actually unstable to decomposition into Si and SiH₄ and should be considered as possible metastable phases. Yet, in this paper, it is demonstrated that a SiH₃ phase with $I4/m$ symmetry is stabilized from 430 to 578 GPa. Also, SiH₂ and SiH turn out to be stable in structures with $I4/mmm$ and $Fm\bar{3}m$ symmetries above 386 and 486 GPa, respectively. Although the estimated T_c is not so high in the $Fm\bar{3}m$ SiH (14 K at 500 GPa) owing to the low hydrogen concentration, T_c reaches 83 K in the $I4/mmm$ SiH₂ at 400 GPa and 88 K in

the $I4/m$ SiH_3 at 450 GPa. Interestingly, these T_c values are rather high in comparison with those estimated for stable SiH_4 phases below ~ 500 GPa.

II. TECHNICAL DETAILS

Ab initio calculations based on the density functional theory are performed within the generalized gradient approximation [29], where the functional form of Perdew, Burke, and Ernzerhof is chosen [30]. Plane-wave basis sets and ultrasoft pseudopotentials [31] are utilized with the use of QUANTUM ESPRESSO [32]. The cutoff radius of the Si pseudopotential is 0.953 Å (with 3s and 3p electrons treated as valence ones) and that of the H pseudopotential is 0.423 Å. The cutoff energy of the plane-wave basis sets is set to 816 eV. The number of \mathbf{k} points is chosen to be greater than $(40 \text{ \AA})^3/v_{\text{cell}}$, where v_{cell} is the volume of the simulation cell. As a smearing function for the occupation around the Fermi energy, a Fermi-Dirac distribution with a temperature of $k_B T = 0.1$ eV is used. Electron-phonon coupling is analyzed by using the density functional perturbation theory [33]. The numbers of \mathbf{k} points and \mathbf{q} points (namely, phonon wave vectors) are chosen to be larger than $(50 \text{ \AA})^3/v_{\text{cell}}$ and $(13 \text{ \AA})^3/v_{\text{cell}}$, respectively, in the calculations of electron-phonon interaction.

The investigation of stable structures is carried out by random structure searches [34,35], where many initial structures are randomly generated and then optimized in order to find out low-enthalpy structures. The number of randomly generated structures ranges from 400 to 3000, depending on the number of atoms and the composition. The \mathbf{k} -point number is decreased to about $(20 \text{ \AA})^3/v_{\text{cell}}$ in the random searches. After several low-enthalpy structures are picked out as candidate structures from the random searches, their structural parameters and enthalpies are refined with the \mathbf{k} -point number increased. Then, for those candidate structures, the zero-point energy of nuclei (ZPE) is estimated to finally determine the lowest-enthalpy structure. The ZPE is calculated within the harmonic approximation, the frozen phonon method being used by making use of PHONOPY [36]. The supercells for the frozen-phonon calculations are constructed such that the number of atoms contained is 64 or larger.

III. STABLE PHASES

Random structure searches have been performed for SiH, SiH₂, and SiH₃ at 200, 300, and 400 GPa. Search cells with 2, 3, 4, 5, and 6 formula units were investigated for all the compositions. The resulting low-enthalpy structures are summarized in the Supplemental Material (Ref. [37]).

It should be mentioned that the above choice of search cells turned out not to be large enough for SiH₃. In fact, the low-enthalpy structures of SiH₃ predicted by the random searches have imaginary-frequency phonons and are dynamically unstable. Therefore, in SiH₃, dynamically stable structures are further looked for manually, where the unstable structures are modified by displacing atoms according to the imaginary-frequency modes with the use of larger cells and then optimized. As a result, there are found out two dynamically stable structures of SiH₃, which have rather large primitive cells: one with 16 formula units below ~ 340 GPa

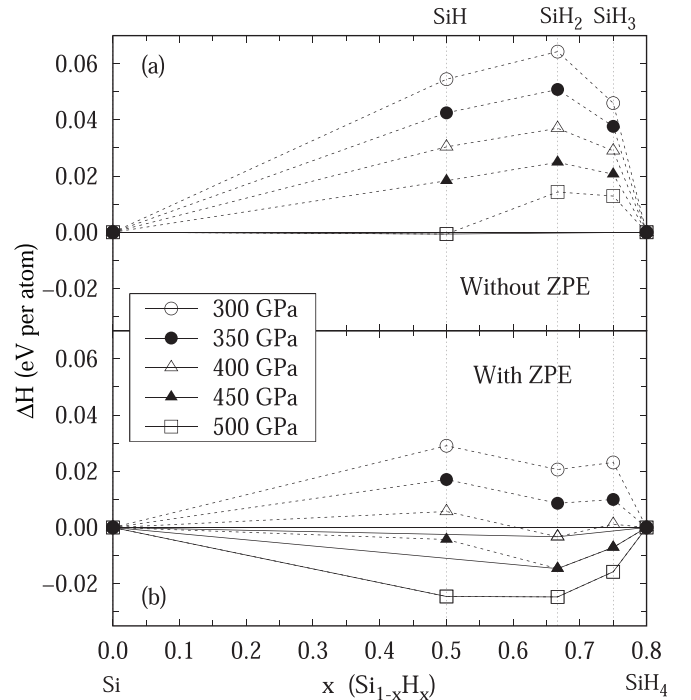


FIG. 1. Relative enthalpy per atom of $\text{Si}_{1-x}\text{H}_x$ as a function of x : (a) without ZPE; (b) with ZPE. Stable compositions are connected with solid lines. See the Supplemental Material (Ref. [37]) for the candidate structures and the structural parameters in SiH, SiH₂, SiH₃, and SiH₄. The enthalpy of Si is calculated for the fcc structure [38].

which has $P2_1/c$ symmetry and the other with 8 formula units above ~ 340 GPa which has $I4/m$ symmetry. This fact might seem to indicate that the above search cells are not large enough even in SiH and SiH₂. However, it should be stressed that the SiH and SiH₂ phases obtained from the random searches have very simple structures as shown later. Usually, such simple structures are not predicted by random searches when search cells are not large enough to accommodate the stable structure. This suggests that the random searches are appropriately performed with the above cell choice in SiH and SiH₂.

In Fig. 1, the relative enthalpy per atom of $\text{Si}_{1-x}\text{H}_x$ is presented as a function of the hydrogen concentration x . The stable compositions are connected with solid lines which correspond to the lower convex envelopes. Without the ZPE, all the subhydrides are unstable to decomposition into Si and SiH₄ at least up to 450 GPa [Fig. 1(a)], though SiH is nearly stabilized around 500 GPa. However, the consideration of the ZPE makes SiH, SiH₂, and SiH₃ possible above 486, 386, and 430 GPa, respectively [Fig. 1(b)]. Actually, as will be discussed later, H atoms are surrounded by more Si atoms in the subhydrides than in SiH₄. This structural property indicates that, in the subhydrides, the Si-H bonding is chemically loose and therefore the average phonon frequency should be low.

Figure 2 shows the comparison of enthalpy between candidate structures in SiH, SiH₂, SiH₃, and SiH₄. In SiH₂, the phase-separated system consisting of Si and SiH₄ is transformed into the homogeneous $I4/mmm$ SiH₂ above 386 GPa. In SiH, the homogeneous phase (namely, the $Fm\bar{3}m$ SiH) appears at a little higher pressures than in SiH₂; this is partly

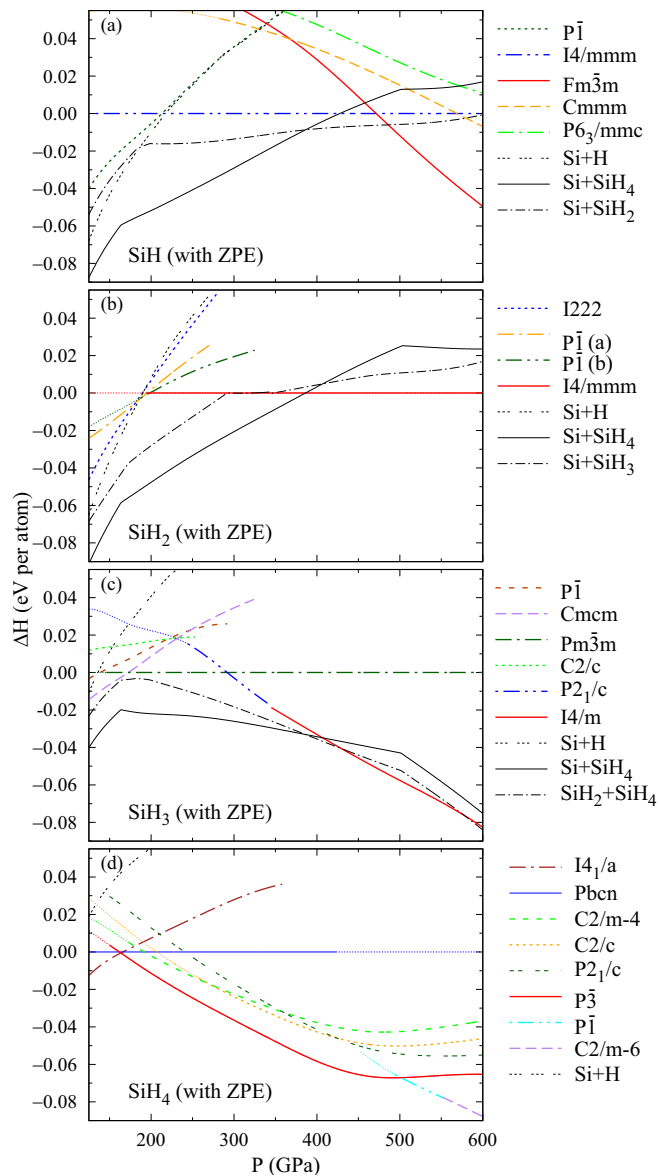


FIG. 2. Comparison of enthalpy between candidate structures in SiH, SiH₂, SiH₃, and SiH₄, where the ZPE is taken into consideration. The enthalpy of Si is calculated for the fcc structure [38], and that of H for the C2/c [39], the Cmca-12 [39], the Cmca [40], and the Cs-IV (*I*_{41/amd} with $c/a > \sqrt{2}$) [41] structures. The thin dotted lines mean that the structures have imaginary-frequency phonons at the pressures, and that the ZPE is calculated by neglecting the unstable phonon modes. See the Supplemental Material (Ref. [37]) for the structural parameters of the SiH, SiH₂, SiH₃, and SiH₄ phases.

due to the stability of the *I*_{4/*mmm*} SiH₂, which forms part of the disproportionated SiH system above 386 GPa. In SiH₃, the homogeneous *I*_{4/*m*} phase becomes stable above 430 GPa, and the system is again decomposed into SiH₂ and SiH₄ above 578 GPa. Note that there have been so far proposed several SiH₃ phases, which are the *P* $\bar{1}$, *C*_{2/*c*}, *Pm* $\bar{3}$ *m*, and *Cmcm* structures [27,28]. However, as already pointed out in Ref. [17], these structures turn out to be thermodynamically unstable to decomposition into Si and SiH₄. Regarding SiH₄, eight structures are compared in Fig. 2(d): the *I*_{41/*a*} [13], the

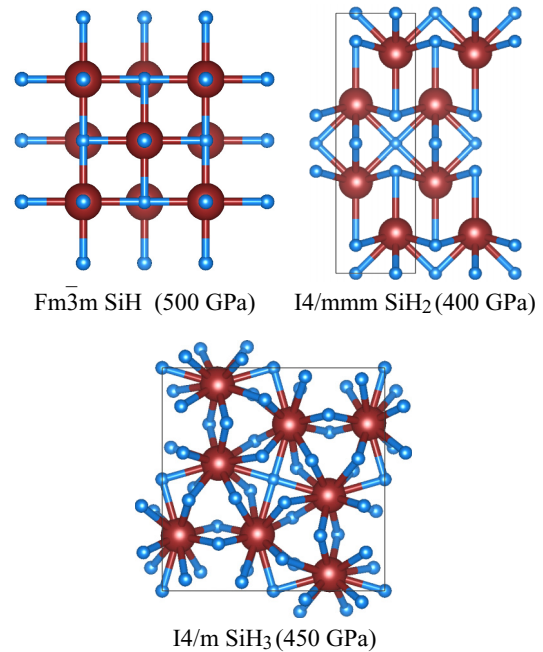


FIG. 3. Structures of the high-pressure phases in SiH, SiH₂, and SiH₃. Solid lines indicate the conventional unit cells. See the Supplemental Material (Ref. [37]) for the structural parameters.

Pbcn [15], the *C*_{2/*m*-4} [17], the *C*_{2/*c*} [13], the *P*_{21/*c*} [16], the *P* $\bar{3}$ [17], the *P* $\bar{1}$, and the *C*_{2/*m*-6} [16] structures, where the *C*_{2/*m*} structure with 4 (6) formula units per primitive cell is denoted by *C*_{2/*m*-4} (*C*_{2/*m*-6}) for the purpose of clarification. In Ref. [17], the *Pbcn* structure was shown to be stable at a very small pressure range from 169 to 175 GPa; in the present calculations, the *Pbcn* structure does not appear as a stable phase. In fact, it is rather difficult to finally determine whether the *Pbcn* structure is possible because the enthalpy of the *Pbcn* structure is quite close to those of the *I*_{41/*a*} and the *P* $\bar{3}$ structures around 170 GPa. In Ref. [16], the *C*_{2/*m*-6} structure is predicted to be stable above \sim 600 GPa. Yet, there are two factors which were not considered in the analysis in Ref. [16]: one is the effect of the ZPE and the other is the *P* $\bar{3}$ structure [17] as a stable phase. By taking account of these two factors, the *C*_{2/*m*-6} structure is found to be possible even below 600 GPa; to be precise, the *C*_{2/*m*-6} SiH₄ is stable above about 550 GPa and its slight modification (the *P* $\bar{1}$ SiH₄) is stable from 503 to 550 GPa. The *C*_{2/*m*-6} SiH₄ has imaginary-frequency phonons below \sim 550 GPa [42], and the analysis of the imaginary-frequency modes leads to finding the *P* $\bar{1}$ SiH₄, which has 12 formula units per primitive cell. Actually, the *P* $\bar{1}$ structure is quite close to the *C*_{2/*m*-6} structure, so that the difference of their enthalpies (without the ZPE) is of the order of 0.1 meV per atom around 500 GPa.

The structures of the high-pressure phases in SiH, SiH₂, and SiH₃ are illustrated in Fig. 3. The *Fm* $\bar{3}$ *m* SiH takes the NaCl-type structure. Since pure Si has the fcc structure at high pressures [38], the *Fm* $\bar{3}$ *m* SiH can be seen as the fcc Si with H atoms absorbed in the octahedral sites. The *I*_{4/*mmm*} SiH₂ also takes a simple structure, which contains only 2 formula units per primitive cell. On the other hand, the *I*_{4/*m*} SiH₃ has a large primitive cell with 8 formula units as mentioned earlier.

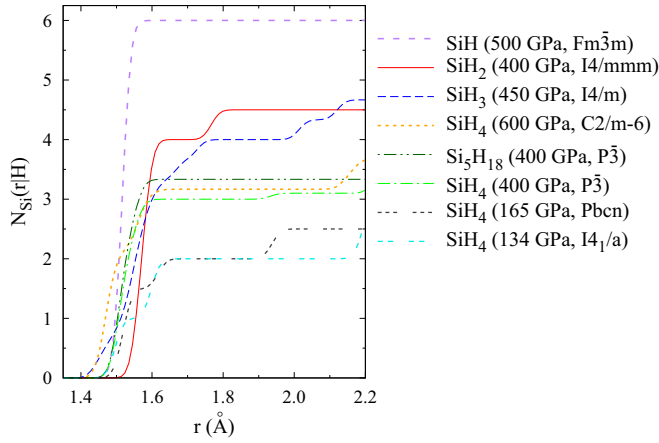


FIG. 4. Number of Si atoms within the distance r from an H atom, $N_{\text{Si}}(r|\text{H})$, which is averaged all over H atoms (see text). The broadening parameter of $N_{\text{Si}}(r|\text{H})$ is set at 0.02 Å. The data for Si_5H_{18} (400 GPa, $P\bar{3}$) is calculated simply by ignoring the relatively isolated H pairs in the $P\bar{3}$ SiH_4 [17].

In SiH_4 at lower pressures, each H atom forms a bridging bond between two Si atoms, and each pair of neighboring Si atoms has the two H-bridging bonds [13,14]. This bonding rule is clearly observed in the $I4_1/a$ SiH_4 and the $Pbcn$ SiH_4 , though the $Pbcn$ structure consists of two-dimensional SiH_4 layers and looks very different from the $I4_1/a$ structure. The bonding rule is changed at higher pressures above ~ 165 GPa (namely, in the $P\bar{3}$ SiH_4) such that an H atom begins to form a bridge between more than two Si atoms. The trend can be found in $N_{\text{Si}}(r|\text{H})$ in Fig. 4, where $N_{\text{Si}}(r|\text{H})$ is the number of Si atoms within the distance r from an H atom being averaged all over H atoms. In other words, by using the radial distribution function between the α th and the β th elements $g_{\alpha\beta}(r)$, $N_{\alpha}(r|\beta)$ is defined by

$$N_{\alpha}(r|\beta) = \int_0^r dr' 4\pi r'^2 n_{\alpha} g_{\alpha\beta}(r'),$$

where n_{α} is the density of the α th element. The value of $N_{\text{Si}}(r|\text{H})$ at the first plateau indicates how many Si atoms surround a single H atom on average. For instance, the first plateau appears at $N_{\text{Si}}(r|\text{H}) = 2.0$ in the $I4_1/a$ SiH_4 (134 GPa) and the $Pbcn$ SiH_4 (165 GPa), where every H atom forms a bridge between two Si atoms. As pressure is raised in SiH_4 , the value of $N_{\text{Si}}(r|\text{H})$ at the first plateau is increased. Indeed, the first plateau can be seen at $N_{\text{Si}}(r|\text{H}) = 3.0$ in the $P\bar{3}$ SiH_4 (400 GPa) and at $N_{\text{Si}}(r|\text{H}) = 3.167$ in the $C2/m-6$ SiH_4 (600 GPa). The $P\bar{3}$ SiH_4 contains an H pair in the primitive cell [17], and the H pair is in fact irrelevant to the H-bridging bonds between Si atoms. Therefore, $N_{\text{Si}}(r|\text{H})$ is recalculated by ignoring the H pair and shown as Si_5H_{18} (400 GPa, $P\bar{3}$) in Fig. 4. This treatment increases the value of $N_{\text{Si}}(r|\text{H})$ at the first plateau from 3.0 to 3.333.

Yet, more significant change in $N_{\text{Si}}(r|\text{H})$ is observed when the composition is changed. In the $I4/m$ SiH_3 (450 GPa), $N_{\text{Si}}(r|\text{H})$ is 4.0 at the first plateau. In the $I4/mmm$ SiH_2 (400 GPa), $N_{\text{Si}}(r|\text{H})$ is likewise 4.0 at the first plateau, but the second plateau with $N_{\text{Si}}(r|\text{H}) = 4.5$ appears at a relatively small r (~ 1.8 Å). Then, in the $Fm\bar{3}m$ SiH (500 GPa), $N_{\text{Si}}(r|\text{H})$

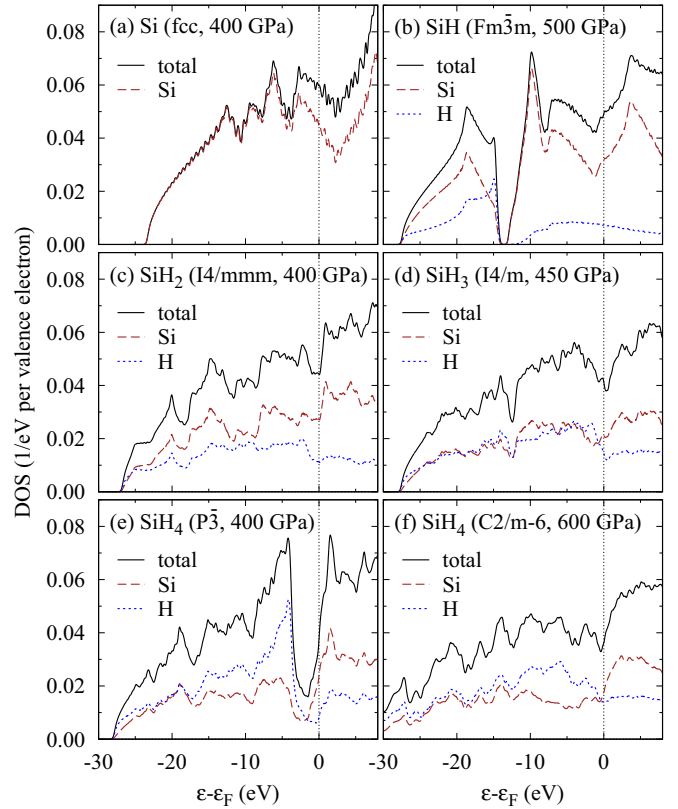


FIG. 5. DOS and PDOS in SiH , SiH_2 , and SiH_3 , where those of the fcc Si [38], the $P\bar{3}$ SiH_4 [17], and the $C2/m-6$ SiH_4 [16] are also shown for comparison. The PDOS of Si (H) is defined as the sum of the contributions from all the Si (H) spheres divided by the number of all the valence electrons.

is 6.0 at the first plateau because H atoms are located on the octahedral sides of the fcc Si. These findings mean that the atoms are arranged more evenly in SiH , SiH_2 , and SiH_3 than in SiH_4 . Apparently, these structural properties in the subhydrides work to lower the ZPE and are crucial for stabilizing them (see Fig. 1). Moreover, in such phases where the atoms are distributed evenly, the electronic structures tend to be delocalized and highly metallic. Hence the structural properties observed in $N_{\text{Si}}(r|\text{H})$ also imply that high- T_c superconductivity is expected in the subhydrides.

IV. ELECTRONIC STRUCTURES AND SUPERCONDUCTING PROPERTIES

The density of states (DOS) and the partial DOS (PDOS) of the SiH , SiH_2 , and SiH_3 phases are presented in Fig. 5, where those of Si and SiH_4 are also shown for comparison. In the $P\bar{3}$ SiH_4 , the DOS shows a clear decrease around the Fermi energy [Fig. 5(e)]. The decrease of the DOS in SiH_4 persists up to 503 GPa, where the $P\bar{3}$ SiH_4 is transformed into the $P\bar{1}$ SiH_4 , whose DOS and PDOS are almost the same as those of the $C2/m-6$ SiH_4 [Fig. 5(f)]. The PDOS in the $P\bar{3}$ SiH_4 shows that the electronic states just below the Fermi energy largely come from H orbitals, while those just above the Fermi energy from Si orbitals. Thus, in SiH_4 , the charge is transferred to some extent from Si atoms to H atoms. The charge

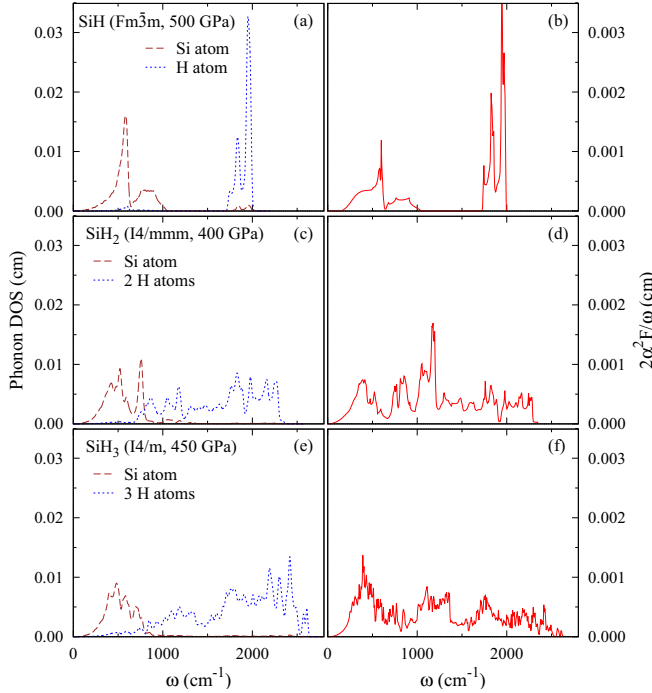


FIG. 6. Phonon DOS (left panels) and Eliashberg function α^2F multiplied by $2/\omega$ (right panels) in SiH, SiH₂, and SiH₃. See Ref. [43] for the details of the computational conditions for the $I4/m$ SiH₃ at 450 GPa.

transfer was previously pointed out for the $I4_1/a$ SiH₄ by Pickard and Needs [13], and is as well seen in the $Pbcn$ SiH₄. Curiously, while the charge transfer is weakened at higher pressures in the $C2/m-6$ phase, it is likewise weakened at lower hydrogen concentrations in the $I4/m$ SiH₃ [Fig. 5(d)] and the $I4/mmm$ SiH₂ [Fig. 5(c)]. Accordingly, the electronic states are delocalized in these subhydrides as conjectured from the structural properties observed in $N_{Si}(r|H)$. Indeed, the DOS curves are relatively close to that of the nearly free electron model in the $I4/mmm$ SiH₂ and the $I4/m$ SiH₃. The $Fm\bar{3}m$ SiH is also a good metal, but the DOS is similar to that of the fcc Si around the Fermi energy. In SiH, because of the low hydrogen concentration, the PDOS of H atoms is a little small at the Fermi energy, and the property implies that electron-phonon coupling is not so large in this system.

Figure 6 presents the phonon DOS and the Eliashberg function α^2F multiplied by $2/\omega$, which is the integrand of electron-phonon coupling parameter λ ($\lambda = \int d\omega 2\alpha^2F/\omega$). In the $Fm\bar{3}m$ SiH, the phonon modes consisting mostly of H motions give rise to very large peaks in $2\alpha^2F/\omega$ just below 2000 cm^{-1} . However, the electron-phonon coupling does not seem to be large as a whole. On the other hand, in the $I4/mmm$ SiH₂ and the $I4/m$ SiH₃, $2\alpha^2F/\omega$ is appreciable over a wide range of pressures. In these two phases, the role of the low-frequency peaks below about 700 cm^{-1} is somewhat important in increasing electron-phonon coupling. The contributions of such low-frequency peaks to electron-phonon coupling are sometimes affected by anharmonicity. For example, anharmonicity is found to drastically suppress the electron-phonon coupling in PdH at one atmosphere [44] and

TABLE I. Superconducting properties of Si, SiH, SiH₂, SiH₃, and SiH₄: electron-phonon coupling parameter λ , logarithmic average phonon frequency ω_{\log} , and superconducting T_c by solving the isotropic Eliashberg equation [48] with $\mu^* = 0.13$. See Ref. [43] for the details of the computational conditions for the $I4/m$ SiH₃ at 450 GPa and the $P\bar{3}$ SiH₄ at 400 GPa.

Phase		P (GPa)	λ	ω_{\log} (K)	T_c (K)
Si	fcc	400	0.137	991	
SiH	$Fm\bar{3}m$	500	0.484	1602	14
SiH ₂	$I4/mmm$	400	0.885	1461	83
SiH ₃	$I4/m$	450	0.934	1413	88
SiH ₄	$P\bar{3}$	400	0.616	1291	28
SiH ₄	$C2/m-6$	600	1.125	1436	127

PtH at 100 GPa [45]. It should be noted, however, that the PdH and PtH phases have imaginary-frequency phonons in the harmonic approximation and anharmonicity is essential to their dynamical stability. When a system is already stable in the harmonic approximation, it seems that anharmonic effects on T_c are moderate. This can be seen, for instance, in the $Im\bar{3}m$ SH₃ and the $Fm\bar{3}m$ LaH₁₀, where theoretical estimates of T_c in the harmonic approximation [4,8] are in good agreement with experimental observations [3,5–7]. As an exceptional case, one might think of the $Pm\bar{3}n$ AlH₃, where anharmonicity is predicted to decrease λ considerably [46]. Yet, in the $Pm\bar{3}n$ AlH₃, the electron-phonon coupling comes only from some specific phonon modes around the X points with low frequencies [47]. Therefore, the electron-phonon coupling strongly depends on how the specific phonon modes react to anharmonicity in the $Pm\bar{3}m$ AlH₃. In contrast, in the SiH₂ and SiH₃ phases, various phonons (including high-frequency phonons) contribute to λ ; that is to say, anharmonic effects on the electron-phonon coupling are averaged all over the Brillouin zone and all over the branches. Thus, by considering the dynamical stability in the harmonic approximation and the significant contributions to λ from various phonon modes, the superconducting properties are expected to be less sensitive to anharmonicity in the silicon subhydrides.

For the SiH, SiH₂, and SiH₃ phases, T_c is estimated by directly solving the isotropic Eliashberg equation. The values of T_c are presented in Table I together with λ and logarithmic average phonon frequency ω_{\log} , where the data of Si and SiH₄ are also shown for comparison. Note that the fcc Si does not show superconductivity at all because λ is very small ($\lambda = 0.137$ at 400 GPa). This clearly shows that the electron-phonon coupling in the hydrides owes a lot to the existence of H atoms, whose $1s$ states strongly interact with proton motions. The estimated T_c is still small in the $Fm\bar{3}m$ SiH (14 K at 500 GPa). Yet, the values of T_c in the $I4/mmm$ SiH₂ and the $I4/m$ SiH₃ are high, reaching 83 K at 400 GPa and 88 K at 450 GPa, respectively. These T_c values are higher than those in SiH₄ at corresponding pressures: T_c in the $P\bar{3}$ SiH₄ is 28 K at 400 GPa or 35 K at 300 GPa according to Ref. [17]. When pressure is raised so that SiH₄ is in the $C2/m-6$ phase, T_c is increased to 127 K at 600 GPa [16]. Such a high T_c is similarly expected above 503 GPa since the structure of the $P\bar{1}$ SiH₄ is very close to that of the $C2/m-6$ SiH₄. However,

the current capability of diamond anvil cells being considered, it seems to be still difficult to experimentally attain such high pressures though it is not impossible. Thus, as a possible way for achieving high- T_c superconductivity in silicon hydride, it might be worth trying to compress silicon and hydrogen in silicon excess conditions.

V. SUMMARY

Dense silicon hydrides have been investigated by using *ab initio* methods, with chief attention being paid to SiH, SiH₂, and SiH₃. The prominent stability of SiH₄ prohibits the other compositions to be thermodynamically stable at lower pressures. Yet the $Fm\bar{3}m$ SiH, the $I4/mmm$ SiH₂, and the $I4/m$ SiH₃ become possible above 486, 386, and 430 GPa, respectively.

The phases of silicon subhydrides predicted here are good metals. While the DOS in SiH₄ shows a clear decrease around the Fermi energy up to 503 GPa, such a decrease of DOS is much smaller in the subhydrides. The estimated T_c values in SiH₂ and SiH₃ reach 83 K at 400 GPa and 88 K at 450 GPa, respectively, which are higher than that in SiH₄ (28 K at 400 GPa). These results in silicon hydrides are similar to those in aluminium and germanium hydrides, where subhydrides AlH [24] and GeH₃ [25] are predicted to have higher T_c than AlH₃ and GeH₄, respectively. All the findings suggest that some other subhydrides are also capable of bringing about high- T_c superconductivity. For example, it might be interesting to investigate subhydrides of gallium, which is close to silicon, germanium, and aluminium on the Periodic Table.

-
- [1] N. W. Ashcroft, *Phys. Rev. Lett.* **21**, 1748 (1968).
 [2] J. J. Gilman, *Phys. Rev. Lett.* **26**, 546 (1971).
 [3] A. P. Drozdov, M. I. Eremets, I. A. Troyan, V. Ksenofontov, and S. I. Shylin, *Nature (London)* **525**, 73 (2015).
 [4] D. Duan, Y. Liu, F. Tian, D. Li, X. Huang, Z. Zhao, H. Yu, B. Liu, W. Tian, and T. Cui, *Sci. Rep.* **4**, 6968 (2014).
 [5] M. Einaga, M. Sakata, T. Ishikawa, K. Shimizu, M. I. Eremets, A. P. Drozdov, I. A. Troyan, N. Hirao, and Y. Ohishi, *Nat. Phys.* **12**, 835 (2016).
 [6] M. Somayazulu, M. Ahart, A. K. Mishra, Z. M. Geballe, M. Baldini, Y. Meng, V. V. Struzhkin, and R. J. Hemley, *Phys. Rev. Lett.* **122**, 027001 (2019).
 [7] A. P. Drozdov, P. P. Kong, V. S. Minkov, S. P. Besedin, M. A. Kuzovnikov, S. Mozaffari, L. Balicas, F. F. Balakirev, D. E. Graf, V. B. Prakapenka, E. Greenberg, D. A. Knyazev, M. Tkacz, and M. I. Eremets, *Nature (London)* **569**, 528 (2019).
 [8] H. Liu, I. I. Naumov, R. Hoffmann, N. W. Ashcroft, and R. J. Hemley, *Proc. Natl. Acad. Sci. USA* **114**, 6990 (2017).
 [9] Z. M. Geballe, H. Liu, A. K. Mishra, M. Ahart, M. Somayazulu, Y. Meng, M. Baldini, and R. J. Hemley, *Angew. Chem. Int. Ed.* **57**, 688 (2018).
 [10] N. W. Ashcroft, *J. Phys.: Condens. Matter* **16**, S945 (2004).
 [11] N. W. Ashcroft, *Phys. Rev. Lett.* **92**, 187002 (2004).
 [12] J. Feng, W. Grochala, T. Jaron, R. Hoffmann, A. Bergara, and N. W. Ashcroft, *Phys. Rev. Lett.* **96**, 017006 (2006).
 [13] C. J. Pickard and R. J. Needs, *Phys. Rev. Lett.* **97**, 045504 (2006).
 [14] Y. Yao, J. S. Tse, Y. Ma, and K. Tanaka, *Eur. Phys. Lett.* **78**, 37003 (2007).
 [15] M. Martinez-Canales, A. R. Oganov, Y. Ma, Y. Yan, A. O. Lyakhov, and A. Bergara, *Phys. Rev. Lett.* **102**, 087005 (2009).
 [16] H. Zhang, X. Jin, Y. Lv, Q. Zhuang, Y. Liu, Q. Lv, K. Bao, D. Li, B. Liu, and T. Cui, *Sci. Rep.* **5**, 8845 (2015).
 [17] W. Cui, J. Shi, H. Liu, Y. Yao, H. Wang, T. Iitaka, and Y. Ma, *Sci. Rep.* **5**, 13039 (2015).
 [18] L. Sun, A. L. Ruoff, C.-S. Zha, and G. Stupian, *J. Phys.: Condens. Matter* **18**, 8573 (2006).
 [19] X.-J. Chen, V. V. Struzhkin, Y. Song, A. F. Goncharov, M. Ahart, Z. Liu, H.-k. Mao, and R. J. Hemley, *Proc. Natl. Acad. Sci. USA* **105**, 20 (2008).
 [20] M. I. Eremets, I. A. Trojan, S. A. Medvedev, J. S. Tse, and Y. Yao, *Science* **319**, 1506 (2008).
 [21] T. A. Strobel, A. F. Goncharov, C. T. Seagle, Z. Liu, M. Somayazulu, V. V. Struzhkin, and R. J. Hemley, *Phys. Rev. B* **83**, 144102 (2011).
 [22] C.-H. Hu, A. R. Oganov, Q. Zhu, G.-R. Qian, G. Frapper, A. O. Lyakhov, and H.-Y. Zhou, *Phys. Rev. Lett.* **110**, 165504 (2013).
 [23] G. Gao, A. R. Oganov, Y. Ma, H. Wang, P. Li, Y. Li, T. Iitaka, and G. Zou, *J. Chem. Phys.* **133**, 144508 (2010).
 [24] K. Abe, *Phys. Rev. B* **100**, 174105 (2019).
 [25] K. Abe and N. W. Ashcroft, *Phys. Rev. B* **88**, 174110 (2013).
 [26] P. Hou, F. Tian, D. Li, Z. Zhao, D. Duan, H. Zhang, X. Sha, B. Liu, and T. Cui, *RSC Adv.* **5**, 19432 (2015).
 [27] X. Jin, X. Meng, Z. He, Y. Ma, B. Liu, T. Cui, G. Zou, and H.-k. Mao, *Proc. Natl. Acad. Sci. USA* **107**, 9969 (2010).
 [28] J. A. Flores-Livas, M. Amsler, T. J. Lenosky, L. Lehtovaara, S. Botti, M. A. L. Marques, and S. Goedecker, *Phys. Rev. Lett.* **108**, 117004 (2012).
 [29] J. P. Perdew, in *Electronic Structure of Solids '91*, edited by P. Ziesche and H. Eschrig (Akademie Verlag, Berlin, 1991), p. 11.
 [30] J. P. Perdew, K. Burke, and M. Ernzerhof, *Phys. Rev. Lett.* **77**, 3865 (1996); **78**, 1396(E) (1997).
 [31] D. Vanderbilt, *Phys. Rev. B* **41**, 7892 (1990).
 [32] P. Giannozzi, S. Baroni, N. Bonini, M. Calandra, R. Car, C. Cavazzoni, D. Ceresoli, G. L. Chiarotti, M. Cococcioni, I. Dabo, A. Dal Corso, S. de Gironcoli, S. Fabris, G. Fratesi, R. Gebauer, U. Gerstmann, C. Gougoussis, A. Kokalj, M. Lazzeri, L. Martin-Samos, N. Marzari, F. Mauri, R. Mazzarello, S. Paolini, A. Pasquarello, L. Paulatto, C. Sbraccia, S. Scandolo, G. Sclauzero, A. P. Seitsonen, A. Smogunov, P. Umari, and R. M. Wentzcovitch, *J. Phys.: Condens. Matter* **21**, 395502 (2009).
 [33] S. Baroni, S. de Gironcoli, A. Dal Corso, and P. Giannozzi, *Rev. Mod. Phys.* **73**, 515 (2001).
 [34] C. J. Pickard and R. J. Needs, *J. Phys.: Condens. Matter* **23**, 053201 (2011).
 [35] K. Abe, *Phys. Rev. B* **96**, 144108 (2017); **98**, 134103 (2018).
 [36] A. Togo, F. Oba, and I. Tanaka, *Phys. Rev. B* **78**, 134106 (2008).

- [37] See Supplemental Material at <http://link.aps.org/supplemental/10.1103/PhysRevB.103.134118> for the candidate structures and their structural parameters.
- [38] R. J. Needs and A. Mujica, *Phys. Rev. B* **51**, 9652 (1995).
- [39] C. J. Pickard and R. J. Needs, *Nat. Phys.* **3**, 473 (2007).
- [40] B. Edwards, N. W. Ashcroft, and T. Lenosky, *Europhys. Lett.* **34**, 519 (1996).
- [41] K. Nagao, H. Nagara, and S. Matsubara, *Phys. Rev. B* **56**, 2295 (1997).
- [42] In the $C2/m-6$ SiH_4 at ~ 550 GPa, imaginary-frequency phonons appear around $\mathbf{q} = (\mathbf{b}_1 - \mathbf{b}_2)/4$ with \mathbf{b}_i being the primitive reciprocal lattice vectors; here, the primitive lattice vectors are chosen as $\mathbf{a}_1 = (\mathbf{a} + \mathbf{b})/2$, $\mathbf{a}_2 = (-\mathbf{a} + \mathbf{b})/2$, and $\mathbf{a}_3 = \mathbf{c}$, where \mathbf{a} , \mathbf{b} , and \mathbf{c} are the conventional lattice vectors with the \mathbf{b} axis being the unique axis (see Ref. [37] for the structural parameters).
- [43] For the calculations of the electron-phonon coupling in the $P\bar{3}$ SiH_4 at 400 GPa and in the $I4/m$ SiH_3 at 450 GPa, the cutoff radius of the H pseudopotential (r_c^H) is increased from 0.423 to 0.529 Å, and the cutoff energy (E_c) is accordingly lowered from 816 to 626 eV. This choice has been made because the structures have relatively large primitive cells and the electron-phonon analysis is quite time consuming. [Although the $C2/m-6$ SiH_4 likewise has a large primitive cell, the H pseudopotential with $r_c^H = 0.423$ Å is used for the system because the target pressure is quite high (600 GPa).] The accuracy of this computational condition is checked by comparing T_c in the $I4/m$ SiH_3 at 450 GPa between the smaller- r_c^H (namely, higher- E_c) and the larger- r_c^H (namely, lower- E_c) calculations, where coarse \mathbf{k} -point and \mathbf{q} -point grids are used: $n_k \sim (45 \text{ Å})^3/v_{\text{cell}}$ and $n_q \sim (10 \text{ Å})^3/v_{\text{cell}}$. The resulting T_c calculated with the smaller r_c^H is 96 K and that with the larger r_c^H is 97 K. The small difference in T_c shows that the error brought about by the choice of $r_c^H = 0.529$ Å and $E_c = 626$ eV is almost negligible even at such high pressures.
- [44] I. Errea, M. Calandra, and F. Mauri, *Phys. Rev. Lett.* **111**, 177002 (2013).
- [45] I. Errea, M. Calandra, and F. Mauri, *Phys. Rev. B* **89**, 064302 (2014).
- [46] B. Rousseau and A. Bergara, *Phys. Rev. B* **82**, 104504 (2010).
- [47] I. Goncharenko, M. I. Erements, M. Hanfland, J. S. Tse, M. Amboage, Y. Yao, and I. A. Trojan, *Phys. Rev. Lett.* **100**, 045504 (2008).
- [48] See, for example, P. B. Allen and B. Mitrović, in *Solid State Physics*, edited by F. Seitz, D. Turnbull, and H. Ehrenreich (Academic Press, New York, 1983), Vol. 37, p. 1.